UC San Diego

UC San Diego Previously Published Works

Title

Advancing use of Cold-formed Steel Framing Systems for Mid-Rise Residential Construction in Seismic Zones via Full-Scale Shake Table Testing

Permalink

https://escholarship.org/uc/item/8p68x1w1

Authors

Hutchinson, Tara

Eladly, Mohammed

Ji, Ruipu

et al.

Publication Date

2026-03-18

Copyright Information

This work is made available under the terms of a Creative Commons Attribution License, available at https://creativecommons.org/licenses/by/4.0/

Peer reviewed

eScholarship.org Powered by the California Digital Library
University of California

Advancing use of Cold-formed Steel Framing Systems for Mid-Rise Residential Construction in Seismic Zones via Full-Scale Shake Table Testing

Tara C. Hutchinson[1], Mohammed Eladly[2], Ruipu Ji[1], Daniel Rivera[1], Fidence Cyizere Rukundo[2], Amanpreet Singh[2], Shokrullah Sorosh[1], Jiachen (Charlie) Zhang[1], Xianzhao Zhang[1], Lynn Padgett[3], Harry Jones[4], Jesse Karns[5], and Benjamin W. Schafer[2]

[1]Department of Structural Engineering, University of California San Diego, La Jolla, CA 92093, e-mail:<tara,r5ji,d3rivera,ssorosh,jiz149,xiz217>@ucsd.edu
[2]Department of Civil and Systems Engineering, Johns Hopkins University, Baltimore, MD 21218, e-mail: <eladly,fcyizer1,amanprs,schafer>@jhu.edu
[3]ClarkDietrich Engineering Services LLC, 330 Greenwood Place, McDonough, GA 30253, e-mail: lynn.padgett@clarkdietrich.com
[4]DCI Engineers, 6363 S.Fiddlers Green Circle, Suite 610, Greenwood Village, CO 80111, e-mail: hjones@dci-engineers.com
[5]MiTek, 555 S Promenade Ave, Corona, CA 92879, e-mail: jkarns@mii.com

ABSTRACT

A capstone 10-story cold-formed steel (CFS) framed building was constructed at the Large High-Performance Outdoor Shake Table at the University of California San Diego (NHERI@UC San Diego). Coined CFS10, this unique, full-scale, building specimen is designed beyond current code-limits with advances in steel sheet sheathed shear walls incorporating high-capacity chord stud detailing proofed in complementary component test programs. This landmark test specimen was designed as an 11.6 m x 6.9 m slice of an archetype CFS-framed residential building. Interior and exterior finishes as well as a wide range of nonstructural systems (stairs, fire sprinkler and gas piping, windows, and doors) were designed and installed in the building. The integrated nonstructural systems add realism to the building and ultimately aid in the opportunity to document the performance of true-to-constructed CFS-framed residential buildings. Uniquely, the building embraces a variety of construction modalities including 2D panelized and 3D volumetric construction methods. Detailing and advances of the later are the subject of a companion paper (Rivera et al., 2026).

Testing of the CFS10 building specimen at the NHERI@UC San Diego shake table was recently completed and involved subjecting the specimen to a suite of 18 increasing intensity multi-directional earthquake motions, followed by execution of two live fire compartment tests. This paper presents an overview of the salient design and construction features of the specimen, the earthquake test protocol and an early impression of the buildings' behavior during the seismic test phase. This is the first publication since testing, with final data processing in progress.

INTRODUCTION

Cold-formed steel (CFS) is a promising material for use in construction of tall residential buildings. Amongst its greatest attributes are its high strength-weight ratio, considerable use of recycled steel content, non-combustible nature, dimensional stability, corrosion resistance, and precision (e.g. Schafer, 2011; SFIA, 2025). CFS has an unprecedented level of consistency compared with most other construction materials, it is therefore easy to prefabricate and mass produce. Its lightweight nature results in components that are easier to handle and erect – leading to innovation in construction. For example, CFS can be constructed by placing individual sticks (studs, track, joists) one-by-one (also referred to as stick framing); by pre-fabricating larger wall and floor components (2D elements, also known as panelized framing); and by constructing volumetric (3D) components (modular construction). Most notably, in moderate-to-high seismic zones, lighter materials lead to reduced seismic forces. Due to advances in code-procedures and construction adoption, CFS has emerged as a popular alternative to wood framing.

In recent years, lightweight structures constructed of load bearing CFS-framing have demonstrated robust structural behavior during system-level shake table testing. Amongst the most notable are full-scale investigations of CFS-framed buildings by Peterman et al. (2016) and Hutchinson et al. (2021). In the former, a 2-story all CFS-framed building was tested at SUNY-Buffalo under increasing intensity multi-directional earthquake simulations; while the later involved a 6-story all CFS-framed building finished with gypsum sheathing tested at UC San Diego, under increasing intensity uni-directional earthquake simulations. Both programs embraced all-CFS gravity and lateral seismic resistant systems, with sheathed (OSB for the former and steel sheet sheathing for the later) shear walls and ledger-framed CFS-joist framed diaphragms adopted. Robust seismic behavior was observed in each of these programs, with overstrength contributions from non-seismically designated components and architectural finishes evident.

Such landmark programs provide much needed system-level experimental data for validation of all-CFS framing systems in moderate-to-high seismic zones. Despite these unique datasets and complementary component experimental and numerical data, the use of CFS framed systems for taller structures [>19.8m (>65ft), or 6-stories] remains prohibited due to code restrictions (e.g. ASCE 7-22, 2022). To contribute to understanding the seismic performance of tall CFS-constructed buildings, a 10-story full-scale CFS-framed building was recently constructed and tested under increasing intensity multi-directional earthquake shaking and post-earthquake live fire testing. Coined CFS10 (cfs10.ucsd.edu), this building specimen was constructed and tested atop the newly upgraded 6-DOF Large High-Performance Outdoor Shake Table (LHPOST6) at the NHERI@UC San Diego Experimental Facility (esec.ucsd.edu), see Figure 1. This unique specimen serves as the capstone effort to the NSF-funded Collaborative Research Program entitled: *Seismic Resiliency of Repetitively Framed Mid-Rise Cold-Formed Steel Buildings (CFS-NHERI)*. CFS-NHERI is a multi-university-industry collaborative effort that intends to advance knowledge of the seismic performance of mid-rise CFS-framed buildings through connection, component, and system experiments complemented with comprehensive numerical modeling.

Design and Construction of the CFS10 Building – The design basis for the CFS10 building was inspired by archetype building designs developed by Torabian et al. (2016). Namely, a total building height of 31.6 m (including a 1.1m parapet), which exceeds the height limitation of 19.8 m set by the current ASCE 7-22 (2022) design standard, was adopted. The building footprint was selected to utilize the entire shake table platen area, with plan dimensions of 11.58m X-direction (north-south) by 6.86m Y-direction (east-west), see Figure 1. Taking a slice of the full building archetype footprint resulted in three wall lines in the Y-direction with two steel sheet-sheathed shear walls along each wall line, and two wall lines in the X-direction, also with two steel sheet-sheathed shear walls, detailed to provide lateral seismic resistance, see Figure 2a-b. This layout resulted in two room-space compartments, and two "balconies", small portions of the adjacent rooms in the archetype. In addition to the load bearing CFS studs and CFS-steel sheathed shear walls, the test building was detailed with gypsum-board-sheathed gravity walls, an exterior face with a stucco-based finish EIFS (exterior insulation and finishing system) on its north side (the south side is a corridor in the full building), and a ledger-framed CFS floor framing system with a dry cementitious panel diaphragm.

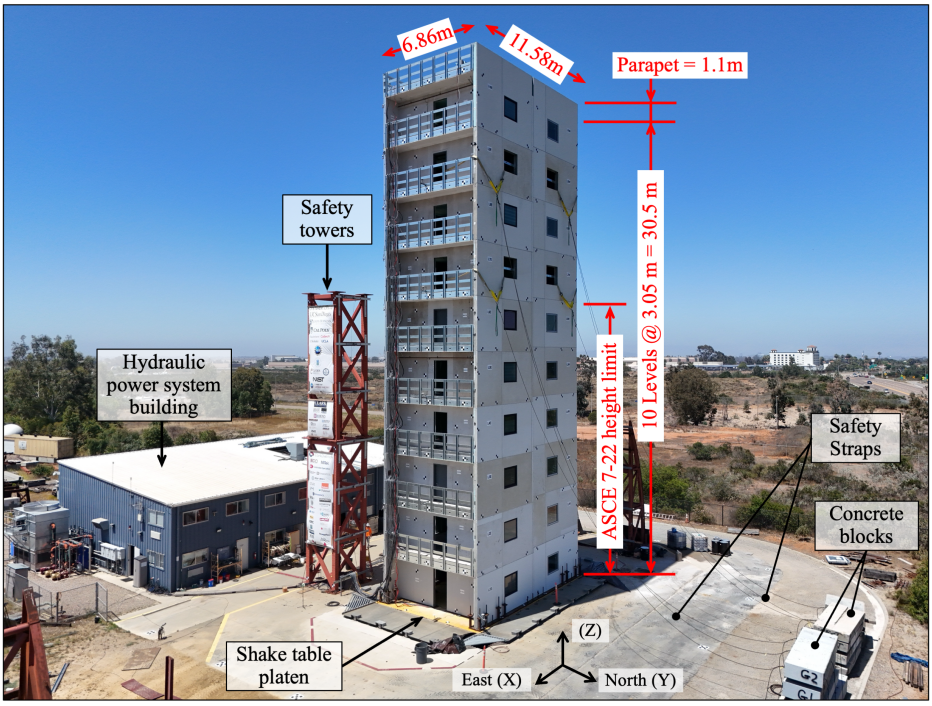
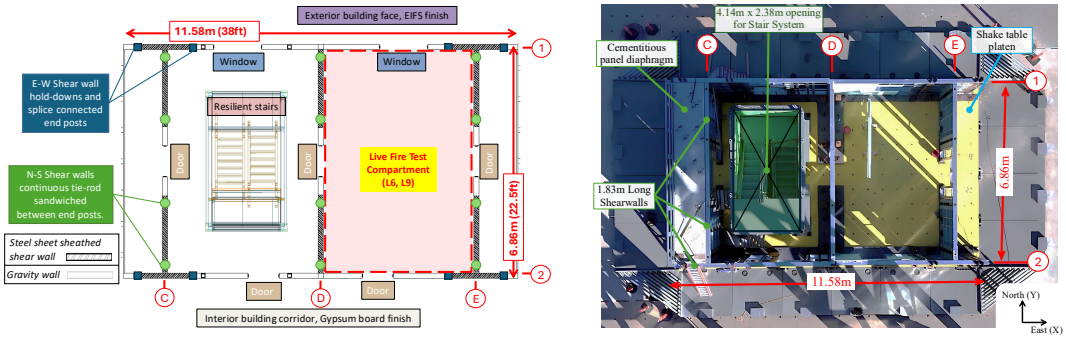


Fig 1. Annotated photograph of the CFS10 specimen, Northeast view

A hypothetical location in a highly active seismic region in Southern California (city of Irvine) with a Site Class C (very dense soil and soft rock) condition was selected as the basis for the building's seismic design. In accordance with ASCE 7-16 (2016) and an assumed Risk Category II, the seismic design parameters were defined as follows: spectral acceleration at short periods, S_S = 1.261 g, spectral acceleration at a period of 1 second, S_1 = 0.452 g, and design spectral accelerations, S_{DS} = 1.009 g and S_{D1} = 0.452 g. The resulting lateral force resisting system of the test building embraced the concept

of Type I shear walls (AISI, 2015) featuring single-sided steel sheet sheathing and ledger framing for floor-to-wall connections. The exception to the use of all CFS structural framing was the detailing of chord studs using HSS tubes on Levels 1-6 for the longitudinal X-direction shear walls (Lines 1 and 2, see Figure 2a), where overturning loads dictated larger capacity requirements and there was a desire not to use large stud packs. In contrast, in the transverse Y-direction, shear walls contain a pair of tie-down subassemblies consisting of tension tie-rods connected by couplers sandwiched between compression posts made of built-up stud packs. The ensuing lateral load resisting system dictates the seismic design parameters R (response modification coefficient), Ω_o (over-strength factor), and C_d (deflection amplification factor) as 6.5, 3.0, and 4.0 respectively per ASCE 7-16 (2016) in its seismic design. Additional details regarding the structural design basis are summarized in Singh et al. (2022, 2024).



(a) (b)

Fig 2. Plan view: (a) cartoon layout and (b) annotated photograph during Level 1 construction.

The building construction explored a variety of methods, namely, conventional stick-framing, panelized (2D), and volumetric (3D) modular construction within one specimen (Figure 3), allowing a unique opportunity to document and compare the efficiency of each, see companion paper by Rivera et al. (2026). Finally, realistic features were incorporated in the building by integrating a wide range of nonstructural components and systems (NCSs). Notably, a 9-story stair system with drift-compatible connections, pressurized gas and fire sprinkler systems, a suspended ceiling system, roof mounted equipment with varied base conditions, select operable doors and windows, and complete interior and exterior finishes to the wall system were incorporated. An overview of the NCSs integrated within the building and their response during the test program will be provided in future publications.

EARTHQUAKE TEST PROGRAM

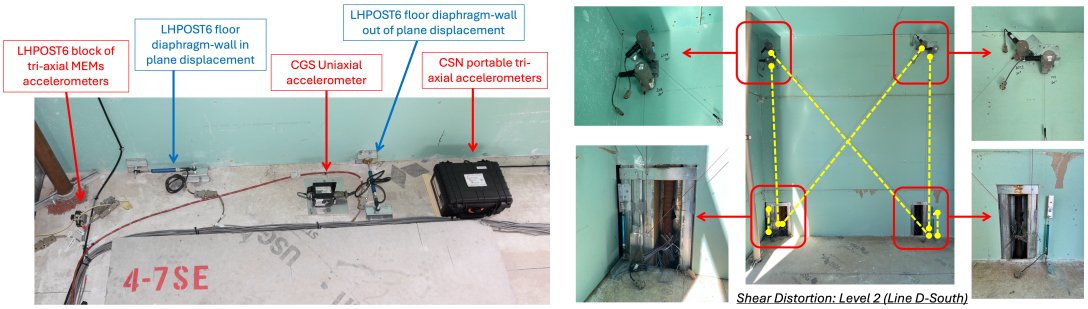
Seismic Instrumentation – To capture the performance of the CFS10 building under the planned earthquake hazard scenarios, multiple forms of data collection were employed. Notably, utilizing LHPOST6 equipment, 730 seismic sensors, 47 synchronized CVI/IP cameras and 17 GoPro cameras were installed throughout the specimen. In addition, in partnership with the California Strong Motion Instrumentation Program (CSMIP) and the Community Seismic Network (CSN), an additional 34 uni-directional and 75 tri-axial accelerometers (CSMIP and CSN, respectively) were distributed throughout the building, see Figure 4. Amongst the 730

seismic sensors, 62% were dedicated to capturing structural behavior (global, walls and diaphragm); while the remaining 38% were allocated to capturing the various nonstructural systems behavior, see Figure 5.

To capture the global behavior of the specimen, absent the potential to provide a fixed reference target for direct displacement measurement to such a tall specimen, an array of unmanned aerial vehicles (UAVs) outfitted with monocular cameras were deployed. For each seismic test, the specimen was monitored by the cameras on the four UAV platforms, each with a different view (plan and three elevations) aimed at capturing structural motions in all degree-of-freedoms (DOFs), see Figure 6. More than 300 reference targets with various types of black-and-white checkerboard patterns were installed to provide image features for detection and tracking. The dynamic response of the structure under seismic excitation can then be extracted by reprojecting image points from UAV imagery to the 3-D world space based on world-to-image point correspondences (Cao et al., 2024; Ji et al., 2025).



Fig 3. Construction methods investigated: (a) stick framing (1D) (Level 1) versus panelized (2D) and (b) modular (3D) (Level 4)



(a) (b)

Fig 4. Example of seismic instrumentation installed: (a) Level 4 diaphragm (southeast corner) and (b) Level 2 shear distortion at wall line D (south)

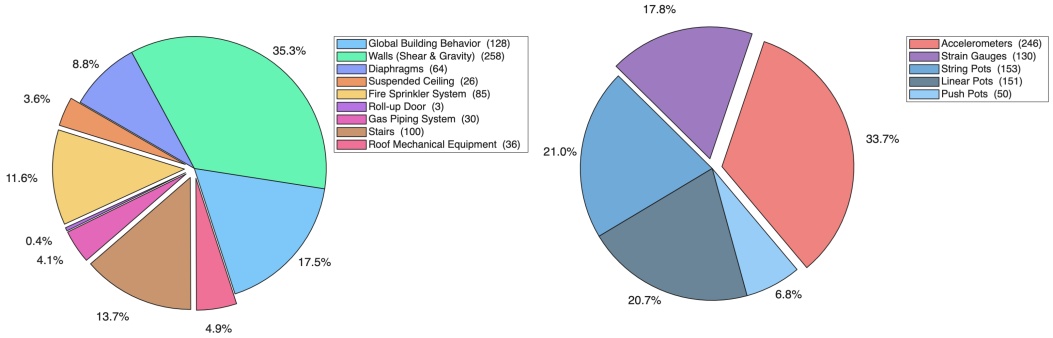


Fig 5. Distribution of LHPOST6 seismic sensors: (left) component (purpose) and (right) sensor type.

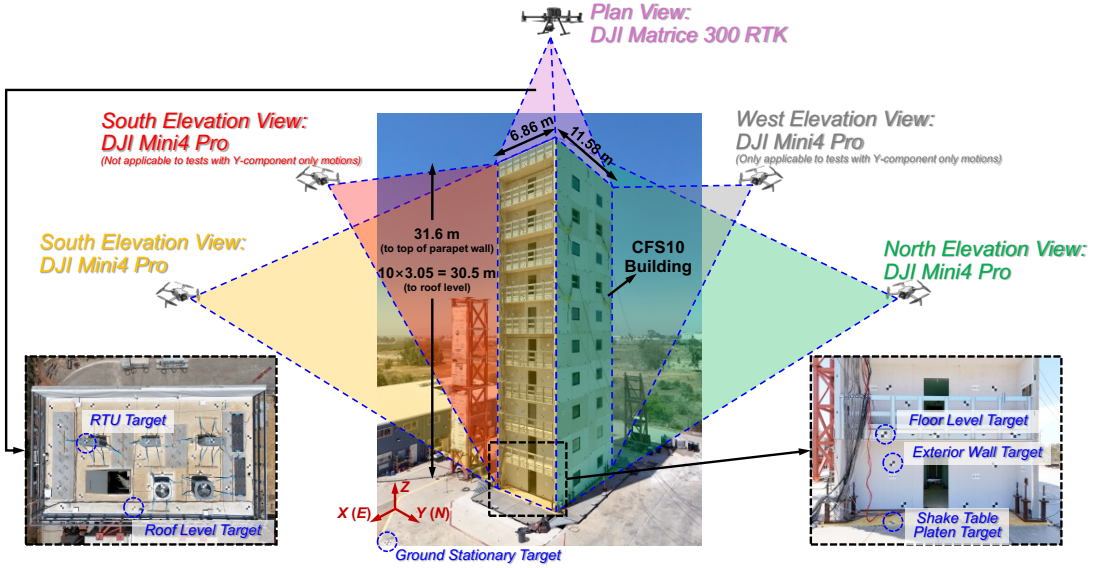


Fig 6. UAV-based structural dynamic response monitoring design.

Test Protocol – In total, 18 earthquake motions of increasing intensity and considering multi-directional input excitations were imposed on the specimen during seven (7) active days of shake table testing. These included 15 service-level earthquakes (SLE), one design-level earthquake (DE) and two risk-targeted maximum considered earthquakes (MCE_R). Two distinct SLE suites (MID1-10 and MID11-15) were designed considering seismological settings characterized by shorter duration far-field and longer duration events, denoted *SLE1* and *SLE2*, respectively. As a result, while

one carry-through increasing intensity motion (1989 Loma Prieta, California – Gilroy Array #3) was utilized across all three hazard levels, a wide range of amplitudes, durations, and directionalities were ultimately imposed on the specimen, see Table 1. Additional details regarding motion selection criteria for this program, including the source selection and scaling procedures adopted, are discussed in Zhang, J. et al. (2024). In addition, to capture the evolution of dynamic characteristics of the building, low-amplitude uni-directional white noise (WN) tests in each orthogonal direction were imposed following each earthquake test. In total, 37 WN tests were conducted, typically with a target root-mean-square (RMS) of 3 or 4%g and a duration of 64 or 160 seconds. It should be noted that during MID1 and the WN immediately before and after, the stairs within the test building were restrained from movement relative to the floor diaphragm at all landings (i.e. "locked"), thus resulting in additional story stiffness contribution. The baseline configuration, i.e. seismically resilient stairs "unlocked", with all mid-landings free to move, was adopted for all subsequent tests.

Table 1. Earthquake test protocol imposed on the CFS10 building. (note: MID = motion identification number, DOF = degree of freedom).

Hazard level	MID	Earthquake event				Input DOF	Components		$D_{5\text{-}95}$ [sec]	PIA_x [g]	PIA_y [g]	PIA_z [g]
		Name, location	Year	M_w	Station		X	Y				
SLE1	1*	Loma Prieta, California	1989	6.9	Gilroy Array #3	XYZ	90°	0°	11.4	0.126	0.122	0.082
	2					XYZ	90°	0°	11.4	0.118	0.114	0.096
	3					X	90°		11.4	0.133	0.041	0.025
	4					Y		0°	6.4	0.042	0.109	0.024
	5	Northridge, California	1994	6.7	LA City Terrace	XYZ	90°	180°	11.9	0.125	0.121	0.081
	6					XYZ	180°	90°	11.9	0.184	0.094	0.084
	7					X	180°		11.9	0.168	0.027	0.023
	8					Y		90°	11.6	0.026	0.093	0.021
	9	Cape Mendocino, California	1992	7.0	Rio Dell Overpass	XYZ	270°	360°	15.3	0.084	0.109	0.099
	10					XYZ	360°	270°	15.3	0.078	0.122	0.151
SLE2	11**	Kahramanmaras, Türkiye	2023	7.8	4611	XYZ	E	N	43.4	0.095	0.075	0.050
	12					XYZ	E	N	43.4	0.117	0.110	0.064
	13	Elbistan, Türkiye	2023	7.5	4611	XYZ	E	N	35.1	0.100	0.061	0.052
	14	Maule, Chile	2010	8.8	Curico Hospital	XY	EW	NS	45.2	0.097	0.091	0.033
	15	Kahramanmaras, Türkiye	2023	7.8	4611	XYZ	E	N	43.4	0.119	0.089	0.063
DE	16	Loma Prieta, California	1989	6.9	Gilroy Array #3	XY	90°	0°	11.4	0.454	0.388	0.014
MCE_R	17	Loma Prieta, California	1989	6.9	Gilroy Array #3	XY	90°	0°	11.4	0.723	0.619	0.016
	18	Cape Mendocino, California	1992	7.0	Rio Dell Overpass	XY	360°	270°	15.3	0.782	0.336	0.025

SLE = service level earthquake, DE = design earthquake, and MCE_R = risk-targeted maximum considered earthquake.
PIA = peak input acceleration (achieved) using shake table platen center of mass accelerometers
$D_{5\text{-}95}$ = significant duration of strong shaking computed as the time interval between 5% and 95% Arias Intensity per original record (max component)
*MID1 was conducted with the stairs in a locked configuration
**MID11 target to 75%SLE

EARTHQUAKE TEST PROGRAM: PRELIMINARY RESULTS

Period Evolution – The vibration periods of the building's first three modes, corresponding to two flexural-dominant modes in each orthogonal direction and one torsional mode, were estimated using one Single Input Multiple Output (SIMO) and one Multiple Output (MO) system identification technique. In the SIMO method, the modal parameters were extracted using the Least Squares Rational Function (LSRF) curve-fitting algorithm (MATLAB, 2022) applied to the Frequency Response Functions (FRFs) of the building. The FRF acts as a transfer function between one input acceleration on the shake table platen and 10 output acceleration measurements recorded on the test specimen at the theoretical center of mass and northwest corner of the building (i.e., considering two uni-directional WN tests and two sensor locations, resulting in a total of 4 input accelerations and 40 output accelerations). In this analysis,

only the flexural-dominant modes that were actively excited were considered. In other words, to estimate the vibration period in the X-direction, data from white noise tests in the X-direction were used, and to estimate the period in the Y-direction, data from white noise tests in the Y-direction were utilized. Figure 7 shows the FRFs from tests WN8 and WN9, which represent the virgin state of the building with the unlocked stair system, and from tests WN35 and WN36, representing the post-earthquake test state of the building. Additionally, the building's dynamic characteristics were determined using the Stochastic Subspace Identification (SSID) technique (Peeters and De Roeck, 2001). In this method, 40 acceleration time histories recorded at the theoretical center of mass and the north-west corner of the building, and four accelerations recorded at the shake table platen are used. Adopting FRF and SSID methods, Figure 8 summarizes the building's periods corresponding to the first three vibration modes throughout the test sequence and the change in the test specimen's period during each WN test relative to WN1 and WN2 tests for "stairs locked" phase and WN8 and WN9 tests for "stairs unlocked" phase. The key observations include the following:

- Computing the building's modal characteristics using the FRF method was effective because the fundamental modes are well separated, and the FRF is well defined due to a high signal-to-noise ratio.
- Periods of the building predicted by the two different system identification techniques are in close agreement.
- SLE-scaled earthquake tests did not alter the vibration period of the building significantly, with the maximum increase of 7% in the first torsional mode. It is worth noting that damage was not visible at the completion of the SLE test suite.
- In contrast, the DE-scaled earthquake increased the vibration period of the first and second flexural modes in the X-direction by approximately 9% and 22%, respectively. Changes in other vibration modes were less than 6%.
- MCE_R tests increased the periods of the first and second flexural modes in the X-direction by approximately 17% and 10%, respectively, and in the Y-direction by approximately 10% and 31%, respectively. The torsional mode period increased by approximately 14%.
- From the virgin state (WN8 and 9) to the post-seismic tests (> MID18, i.e. post-MCE_R), the building's first flexural period increased by as much as 35 and 18% in the X and Y-directions, respectively. The torsional period increased by 23%.

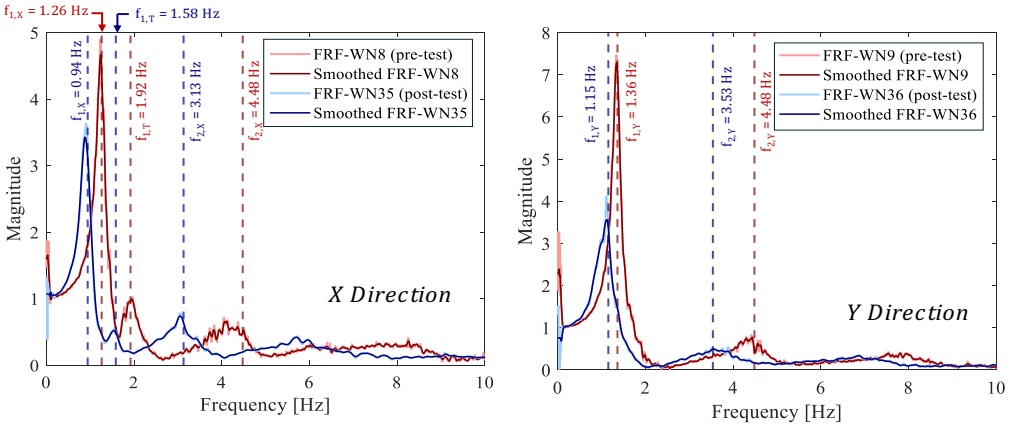


Fig 7. Frequency response function (FRF) using WN8 and WN9 (virgin state), and WN35 and WN36 (post-seismic test state). Note that subscript T refers to the torsional mode.

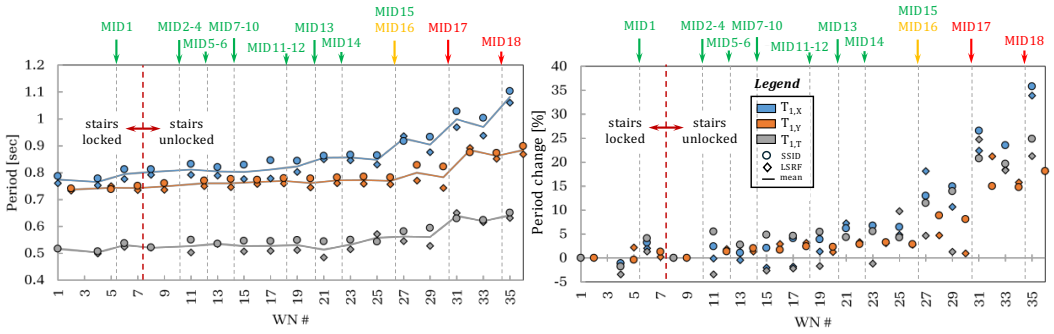


Fig 8. Period evolution of the specimen for the first three fundamental modes.

Peak Acceleration Response – The peak floor acceleration profile with height in a building is an important indicator of the seismic demand during earthquake shaking. Figure 9 presents the peak floor acceleration (PFA) profile considering the SLE suites (part a,b) and the DE+ (DE and MCE_R tests, parts c,d), as measured at the center of mass of the building. The SLE-scaled motions are separated by suites SLE1 (short duration, with $D_{5\text{-}95} < 15$sec) and SLE2 (long duration, with $D_{5\text{-}95} > 30$sec). Under these two suites, it is notable that the longer duration shaking expresses larger PFAs within the upper floors in the X-direction, while the Y-direction consistently reports lower PFAs during the long duration tests. The largest PFA at the center of mass during both SLE suites was 0.44g, measured at the roof in the X-direction. PFA profiles during the final MCE_R test (MID18) were lower than those of the DE-scaled (MID16) test at select floor levels in the Y-direction, indicating that nonlinear response was observed at select floors. The largest PFA at the center of mass during the DE and above-scaled tests was 2.02g, reported at the roof in the X-direction. Higher mode effects are evident in the measured profiles and manifest in the form of larger PFAs for select lower floors (reversals at mid-height) during both SLE and DE+ tests.

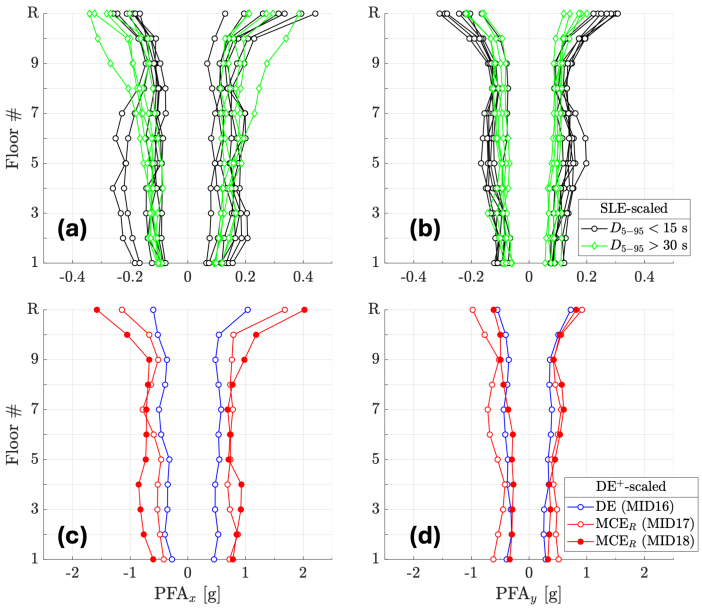


Fig 9. Peak floor acceleration profile during the: (a, b) SLE-scaled suites, considering short and long-duration test motions and (c, d) DE and MCER-scaled tests. Parts (a, c) present the X-direction response, while parts (b, d) present the Y-direction response.

It is also useful to normalize the peak floor acceleration by the achieved peak input acceleration (PIA), see Figure 10. This plot provides individual circles along with the light grey lines (linearly connecting floor-floor) to represent the PFA/PIA from an individual ground motion. The solid red line indicates the geometric mean of the PFA/PIA results from all tests at each floor. In the X-direction, the maximum average PFA/PIA ratios were 2.39 (SLE), 2.07 (DE), and 2.24 (MCE_R). In the Y-direction, the corresponding averages were 2.69, 1.87, and 2.23. These maxima consistently occurred at the roof, where the building's whipping action led to greater acceleration amplification. Compared with the SLE and MCE_R cases, the DE case exhibited smaller roof-level amplification. However, this result may not be statistically robust, as it is based on only one DE test.

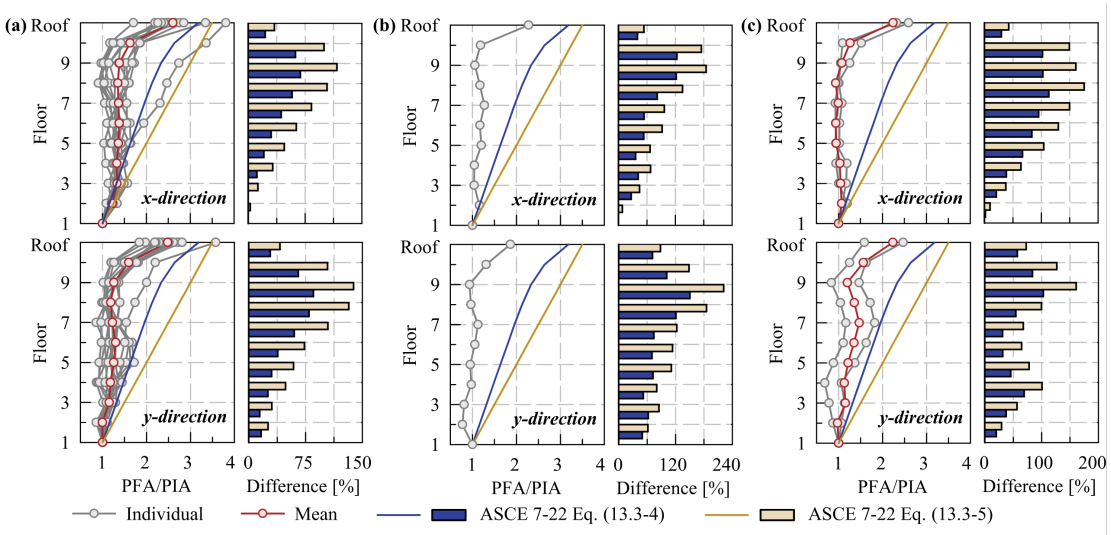


Fig 10. Acceleration amplification factor profile (PFA / PIA = peak floor acceleration / peak input acceleration) under: (a) service-level earthquakes (SLE), (b) design earthquake (DE), and (c) risk-targeted maximum considered earthquakes (MCE_R). Computed using the center of mass accelerometers and compared with ASCE 7-22 (2022).

ASCE 7-22 (Chapter 12, 2022) provides two alternative equations for calculating acceleration amplification factors along the height of a building. The fundamental-period-independent method (Equation 13.3-5), assumes a linear acceleration amplification profile, ranging from 1.0 at the ground level to 3.5 at the roof level. The fundamental-period-dependent method (Equation 13.3-4), introduced in the latest edition, aims to improve prediction accuracy by considering the building's fundamental period, which is calculated using the code-based formula as 0.63 sec (independent of building direction). Figure 10 includes these two code-based profiles and the difference in bar chart format with the mean measured PFA/PIA values. In general, both code-based equations provide conservative predictions of acceleration amplification, with the most conservative result typically occurring at floor 9, except for the x-direction amplification under the MCE_R case, where floor 8 produced a more conservative value. Using Equation (13.3-5), the predicted acceleration amplification was conservative by up to 127%, 220%, and 193% under SLE, DE, and MCE_R motions, respectively. The period-dependent Equation (13.3-4) consistently observes smaller

(bit still substantial) differences with the measured values, with corresponding maximum conservatism of 77%, 149%, and 127%. An exception is noted during MID13 (SLE2-suite), where Equation (13.3-4) fails to reliably predict X-direction acceleration amplification above the fifth floor while Equation (13.3-5) performs better in this range, but loses reliability beyond the ninth floor.

Local Response – Chord members were instrumented with uni-axial strain gages to capture the transient strain amplitude of shear wall perimeter hollow structural sections (HSS) (wall lines 1 and 2) and tie-rod elements (wall lines C, D, and E). A sample of the measured dynamic strain histories are provided in Figure 11a-b during the final MCE_R test (MID18). The comparison in part (a) overlays sensor SF01-17Z (HSS at story 1) and SF06-09Z (HSS at story 6). This plot reveals notable differences in strain magnitude, with the peak measured in the lower story, and approaching 21%ε_y, approximately 1.15 times the magnitude observed at level 6. Similarly, part (b) illustrates an even more pronounced difference between tie-rod responses comparing a tie-rod at level 1 (SF01-01Z), which exhibited peak strains of approximately 20%ε_y, while the tie-rod element at level 10 (SF10-01Z) maintained strains below 2%ε_y, representing an order-of-magnitude difference. A synthesis of maximum strain amplitudes across all 18 tests, categorized by seismic hazard level is provided in part c. These measurements indicate that monitored members maintain strains below 10% of their yield strain, indicating elastic behavior with minimal potential for damage or permanent deformation during all SLE tests, while during the DE-level test modest demands of 11% and 15%ε_y, for the tie-rod and HSS, respectively were recorded. The MCE_R-level test responses produced larger demands, with peak strains reaching 20% ε_y for tie-rods and 27%ε_y for HSS members. These strain amplitudes in chord studs are an anticipated and a welcome outcome, as they are capacity protected elements, therefore at MCE_R-levels, it is desired that damage occurs in other elements.

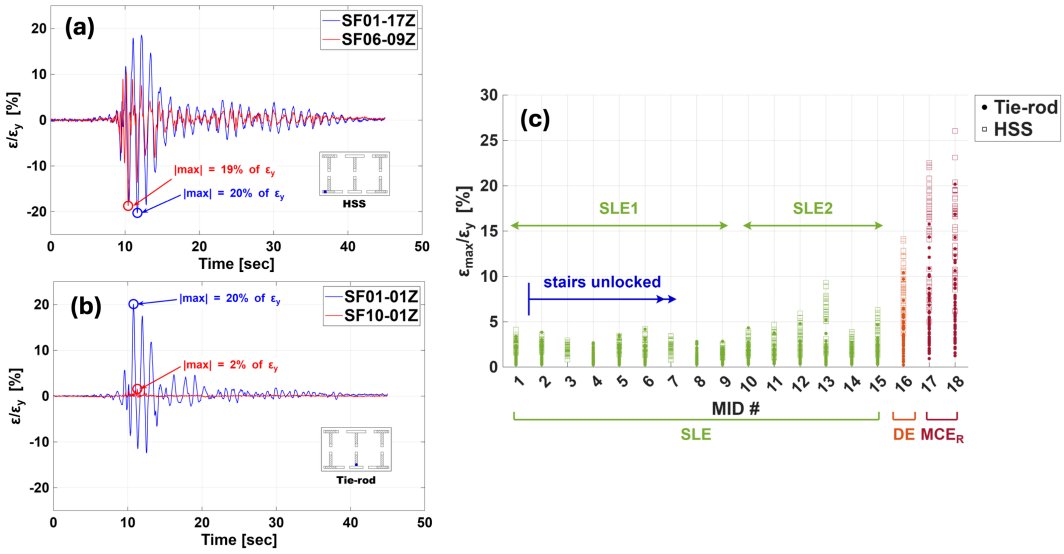


Fig 11. Measured strain on HSS and tie-rod members at the end of shearwalls: (a,b) dynamic histories during MID18, and (c) synthesis of all maximum (transient) strain measured across all tests. Values normalized by the member yield strain.

CONCLUDING REMARKS

A landmark 10-story cold-formed steel (CFS) building was constructed at the large high-performance outdoor shake table at UC San Diego. This unique, full-scale, building specimen is designed beyond current code-height limits with advances in steel sheet sheathed shear walls and unique chord stud details proofed in complementary component test programs. This paper provides a summary of the specimens' salient design and construction features, the seismic instrumentation and test protocol, and preliminary measured earthquake response results. Measured results discussed herein indicate that after 18 simulated earthquakes, two of which were MCE_R-level target scaled, a maximum period elongation in the flexural mode of approximately 35%, with peak floor accelerations of 2g at the roof; and maximum strains in chord stud members < 30% of the yield strain. Peak floor acceleration profiles clearly articulate higher mode effects in this tall building and indicate possible directions for improvements with ASCE7's current design acceleration amplification ratios.

Important to note, though not discussed due to brevity in the present paper, physical damage post DE and post-MCE_R tests was moderate and readily repairable, demonstrating the systems seismic resilience. Features observed include edge fastening damage to finish sheathing, minor crushing and EIFS exterior finish damage, particularly surrounding window openings, mud/tape damage, and one instance of a detached tie-rod at its coupler. Note that no repair actions were taken during the earthquake test sequence. Importantly, residual drift of the building was negligible and continued functionality of all nonstructural systems installed were observed. Future work by the team will explore in greater depth the specimens' measured response, correlating with salient observed damage and computational models. This unique dataset will be used to provide important benchmark comparisons with numerical modeling methods, while also guiding in advancing code-based design of cold-formed steel in mid-rise and tall-building construction.

ACKNOWLEDGEMENTS

The CFS10 project is a collaborative research project, with support through the National Science Foundation (NSF) grants CMMI 1663569 and CMMI 1663348, project entitled: Collaborative Research: Seismic Resiliency of Repetitively Framed Mid-Rise Cold-Formed Steel Buildings and numerous other federal/state and industry partners. A complete list of all sponsors/partners to the CFS10 program may be found at: cfs10.ucsd.edu/sponsors-partners. The efforts of all undergraduate and graduate students and visiting scholars listed at (cfs10.ucsd.edu/people) as well as the LHPOST6 facility staff (esec.ucsd.edu/about/personnel) are greatly appreciated. Findings, opinions, and conclusions are those of the authors and do not necessarily reflect those of the sponsoring organizations.

REFERENCES

ASCE7-16. (2016). Minimum Design Loads and Associated Criteria for Buildings and Other Structures. Standard ASCE/SEI 7–16 (Structural Engineering Institute of American Society of Civil Engineers).

ASCE7-22. (2022). Minimum Design Loads and Associated Criteria for Buildings and Other Structures. Standard ASCE/SEI 7–22 (Structural Engineering Institute of American Society of Civil Engineers).

Cao, P., Ji, R., Ma, Z., Sorosh, S., Lo, E., Norton, T., Driscoll, J., Wang, X., Hutchinson, T., Pei, S. and Kuester, F., (2024). "UAV-Based Video Analysis and Semantic Segmentation for SHM of Earthquake-Excited Structures." *Proceedings of the 18th World Conference on Earthquake Engineering (WCEE2024)*, Milan, Italy.

Hutchinson, T.C., Wang, X., Hegemier, G., Kamath, P., and Meacham, B. (2021). "Earthquake and post-earthquake fire testing of a midrise cold-formed steel-framed building. I: Building response and physical damage," *ASCE Journal of Structural Engineering*. 147(9). doi: 10.1061/(ASCE)ST.1943-541X.0003097.

Ji, R., Sorosh, S., Lo, E., Norton, T.J., Driscoll, J.W., Kuester, F., Barbosa, A.R., Simpson, B.G., Hutchinson, T.C. (2025). "Application Framework and Optimal Features for UAV-Based Earthquake-Induced Structural Displacement Monitoring." *Algorithms*: 18(66). doi.org/10.3390/a18020066.

MATLAB documentation (R2022). The MathWorks, Inc. https://www.mathworks.com/help/matlab/

Peterman, K.D., Stehman, M.J., Madsen, M.J., Buonopane, S.G., Nakata, N., and Schafer, B.W. (2016). "Experimental seismic response of a full-scale cold-formed steel-framed building. I: System-level response." *ASCE Journal of Structural Engineering*. 142(12). doi: 10.1061/(ASCE)ST.1943-541X .0001577.

Peeters B. and De Roeck, G. (2001). Stochastic system identification for operational modal analysis: a review. *Journal of Dynamic Systems, Measurement, and Control*. 123 (4):659-667. doi.org/10.1115/1.1410370

Rivera, D. Zhang, J., Singh, A., Ji, R., Sorosh, S., Eladly, M., Cyizere Rukundo, F., Rivera, D., Ellis, M., Padgett, L., Jones, H., Karns, J., Stewart, D., Schafer, B.W., and Hutchinson, T.C. (2026). "Investigating Construction Methods in a Landmark 10-story Cold-Formed Steel Residential Building Specimen Shake Table Test Program." *8th Residential Building Design & Construction Conference*. Pennsylvania Housing Research Center. March 18-19.

Schafer, B.W. (2011). "Cold-formed steel structures around the world: A review of recent advances in applications, analysis and design." *Steel Construction*, 4(3):141-149, doi: 10.1002/stco.201110019.

SFIA (Steel Framing Industry Association) (2025). "Advantages of using cold-formed steel framing." Accessed on June 10, 2025 at: https://www.cfsteel.org/advantages-of-cold-formed-steel-framing.

Singh, A., Hutchinson, T. C., Torabian, S., Schafer, B. W., Peterman, K. D., Padgett, L., and Jones, H. (2022). "Structural Design Narrative of the CFS-NHERI 10-Story Test Building for Multi-Dimensional Shake Table Testing." *Proceedings of the Cold-Formed Steel Research Consortium Colloquium 2022*, Baltimore, MD, USA.

Singh, A., Zhang, J., Rivera, D., Eladly, M., Jones, H., Kovac, A., Padgett, L., Rivera, D., Smith, K., Torabian, S., Peterman, K. D., Schafer, B. W., and Hutchinson, T. C. (2024). "CFS-NHERI 10-Story Building Shake Table Test Specimen: Design Updates." *Proceedings of the 18th World Conference on Earthquake Engineering (WCEE2024)*, Milan, Italy.

Torabian, S., Nia, Z., and Schafer, B.W. (2016). "An archetype mid-rise building for novel complete cold-formed steel buildings." *Proceedings of the Wei-Wen Yu Int. Specialty Conf. on Cold-Formed Steel Structures*, Baltimore, MD, USA, Nov. 9-10

Zhang, J., Singh, A., Eladly, M., Marcinek, S., Guha, S., Peterman, K.D., Schafer, B.W., and Hutchinson, T.C. (2024). "Ground motion selection and scaling considerations for the CFS-NHERI capstone 10-story building specimen." *Proceedings of the 18th World Conference on Earthquake Engineering (WCEE2024)*, Milan, Italy.